LONG-TERM EVOLUTION OF THE NORTH ANATOLIAN FAULT: NEW CONSTRAINTS FROM ITS EASTERN TERMINATION

Aurélia Hubert-Ferrari [1,2], Geoffrey King[3], Jérome Van Der Woerd [4], Igor Villa [5], Erhan Altunel [6], Rolando Armijo [3]

1-Institut de Géologie, Université de Neuchâtel, rue Émile Argand 11, CH-2007 Neuchâtel, Switzerland,

2- Now at Section de Sismologie, Observatoire Royal de Belgique, rue circulaire 3, B-1180 Brussels, Belgium; tel: 00 32 2 790 39 18, fax: 00 32 2 373 03 39, aurelia.ferrari@oma.be.

3- Laboratoire de Tectonique, Institut de Physique du Globe de Paris, UMR, 4 place Jussieu, Paris, 75252 Cedex 05, France.

4- IPGS-EOST, UMR CNRS/ULP 7516, 5, rue Rene Descartes, Strasbourg, 67084 Cedex, France.

5- Institute of Geological Sciences, University of Bern, Baltzerstrasse 1-3, CH-3012 Bern, Switzerland.

6- Dept. of Geology, Engeneering Faculty, Osmangazi University, Eskisehir, Turkey.

Number of words of text (including abstract, excluding references and figure caption): 4748

Number of references: 86

Number of table: 2

Number of Figures: 11

Abbreviated title: Long-term evolution of the North Anatolian Fault

Abstract

The deformation and ^{40}Ar-^{39}Ar dating of recent volcanism that remarkably sits across the North Anatolian Fault eastern termination in Turkey, together with previous studies, put strong constraints on the long-term evolution of the fault. We argue that after a first phase of 10 Ma, characterized by a slip rate of about 3 mm/yr, and during which most of the trace was established, the slip rate jumped to about 20 mm/yr on average over the last 2.5 Ma, without substantial increase of the fault length. The transition correlates with a change in the geometry at the junction with the East Anatolian Fault that makes the extrusion process more efficient.

The right-lateral North Anatolian Fault (NAF), together with the conjugate East Anatolian Fault (EAF), accommodates the westward extrusion of the Anatolian block toward the Aegean Subduction Zone (Fig. 1; McKenzie 1972, Tapponnier 1977). This process started most probably 12 Ma ago during a late phase of collision between Arabia and Eurasia (Dewey *et al.* 1986; McQuarrie *et al.* 2003) characterized by the uplift of the Anatolian Plateau, the end of marine sedimentation (Gelati 1975; Şengör *et al.* 1985), the onset of volcanism in eastern Anatolia (Yılmaz *et al.* 1987; Pearce *et al.* 1990) and the onset of motion of the North Anatolian Fault (Şengör *et al.* 1985; Barka 1992). Indeed biostratigraphic data unequivocally constrain a Late Miocene age for all basins located along the North Anatolian eastern strand (see Şengör *et al.* (2005) review). Some still propose a later initiation time around 5±2 Ma (Barka & Kadinsky-Cade 1988; Bozkurt & Koçyiğit 1996; Bozhurt 2001). The present-day kinematics of the extrusion, constrained by GPS measurements (McClusky *et al.* 2000; Reilinger *et al.* 2006), shows that deformation is localized along a single narrow zone and that the internal deformation of Anatolia though existing (Tatar *et al.* 1996; Gürsoy *et al.* 1997; Jaffey *et al.* 2004) is negligible (Fig. 1). The present geodetic slip rate of the North Anatolian Fault (22±3 mm/yr: McClusky *et al.* (2000); 24±1 mm/yr: Reilinger *et al.* (2006) is not significantly different from its Holocene slip rate (18.5±3.5 mm/yr; Hubert-Ferrari *et al.* (2002)) deduced from offset geomorphological markers. The study of the offset morphology at a wide range of scales (Hubert-Ferrari *et al.* 2002) suggests that deformation has remained localized along the present fault zone for several million years. Barka & Hancock (1984) further suggest that a broad right-lateral shear zone was existing before deformation fully localized in early Pliocene time on the present strand of the North Anatolian Fault. The present North Anatolian Fault has also a nearly uniform total displacement of ~85 km along most of the fault (Armijo *et al.* 1999; Bozkurt 2001; Westaway & Aeger 2001; Hubert-Ferrari *et al.* 2002; Şengör *et al.* 2005) and is thus similar to a transform boundary. The

total displacement of the North Anatolian Fault, together with the age of the fault (12 Ma), yields an average geological slip rate of 7 mm/yr.

We focus on the Karliova Triple Junction area, where the eastern extremity of the North Anatolian Fault joins the East Anatolian Fault. This pivotal region marks the transition between the continental shortening to the east and the extrusion regime to the west. In addition recent volcanism covers entirely the region and provides ideal chronological markers to record deformation. By mapping the active faults and their offsets, and by characterizing the relationship between faulting and volcanism, we propose that the extrusion process has evolved with time, with two distinct phases characterized by very different slip rates. Interestingly, the Triple Junction (TJ) evolution can be approximated by a simple plate-tectonic model.

Active Faulting at the Anatolia-Eurasia-Arabia Triple Junction

We have established a detailed map of the three main fault systems - the North Anatolian Fault, the Varto Fault, and the East Anatolian Fault- relevant to the triple junction deformation combining Spot images analysis and fieldwork (Figs. 2-5).

At its eastern extremity the North Anatolian Fault can be divided in 4 main segments (Fig. 2). To the west, a first segment of the North Anatolian Fault strikes N125°E and ends at the eastern extremity of the Erzincan basin. This is a complex basin (Barka & Gülen 1989; Fuenzelida *et al.* 1997; Hubert-Ferrari *et al.* 2002), with the left-lateral Ovacık fault terminating southward (Westaway & Aeger 2001). The seismic behavior of the North Anatolian Fault appears to be decoupled on both sides of this major discontinuity (Hubert-Ferrari *et al.* 2002). East of the Erzincan basin a second strait segment extends for 80 km with a N110°E strike to a small pull-apart near Yedisu. East of Yedisu, the faulting geometry is typical of damage fault pattern occurring at the tip of strike-slip fault with slightly more diffuse deformation combining fault branching, horsetail and reverse faulting (Kim & Sanderson 2006). A third segment of the North Anatolian Fault splits, about 10 km south-east of Yedisu, in different curved strands

that ruptured in 1949 (Ambraseys 1988). This segment forms a large horsetail with normal faulting deforming the eastern flank of the Turna Mountain until the East Anatolian Fault. Farther northeast, a fourth segment extends over 30 km to the Triple Junction and accommodates almost only strike-slip motion as shown in Fig. 3 and by focal mechanisms of earthquake of magnitude M>5.5 (Fig. 2). The third and fourth segments form a restraining step-over. Secondary folding parallel to the Periçay River occurs just north of the last segment of the North Anatolian Fault.

East of the Triple Junction the Varto fault system extends over 50 km forming a large motly extensional horsetail. Most of the deformation is localized on the Main Varto Fault that is in strait continuation of the fourth segment of the North Anatolian Fault. This main strand, located exactly at the foot of the Bingöl half-caldera, accommodates mostly strike-slip faulting though partly hidden by landslides (Fig. 4). In 1966, the Varto M=6.8 earthquake (Wallace 1968; Ambraseys & Zatopek 1968) ruptured its eastern part with aftershocks having thrusting mechanism. More diffuse strike-slip and normal deformation exists south of the Main Varto Fault, with a clear southward decreasing gradient of deformation. The network of secondary faults in the Varto horsetail is at a slight angle to the Main Varto Fault; most splay from the Triple Junction, though some splay from the East Anatolian Fault just southeast of the town of Karliova (Fig. 6). The Varto horsetail is also associated with fissure-fed lava flows and intrusion located mostly along faults. The largest intrusions form significant volcanic domes elongated along bounding faults (Figs. 4-5). South of the town of Varto the fissural volcanism cross-cuts older volcanic product related to the Bingöl half-caldera (Buket & Görmüş 1986; Buket & Temel 1998). Significant shortening in the Triple Junction area occurs only 20 km south of Varto along the Muş fold-and-thrust belt (Fig. 2; Şengör *et al.* 1985; Dewey *et al.* 1986).

At the Triple Junction, the East Anatolian fault ends against the North Anatolian and Main Varto Fault systems. Its last 75 km segment smoothly bends eastward as it approaches the Triple Junction. It ruptured

near Bingöl during a M=6.9 earthquake in 1971 (Arpat & Şaroğlu 1972; Seymen & Aydin, 1972). The recent M=6.4 earthquake in May 2003 ruptured a minor conjugate fault (Orgulu *et al.* 2003), probably related to the major change in strike of the East Anatolian Fault near the town of Bingöl (Figs. 1, 4). Near the town of Goynuk the East Anatolian Fault forms a small short-cut pull-apart associated with lacustrine sediments intercalated with lavas of the Turna Mountain and with lignite deposits (Fig. 7).

Recent volcanism at the Anatolia-Eurasia-Arabia Triple Junction

The most salient feature of the Triple Junction is the presence of widespread recent volcanism (Figs. 2, 6a; Dewey *et al.* 1986) that has spectacularly recorded the cumulated deformation.

Along the North Anatolian Fault, we are able to reconstruct a single volcanic edifice from two offset structures (Fig. 6). The first structure, neatly cut to the south by the Main Varto Fault, is the Bingöl half-caldera east of Karliova. The second structure, cut to the north by the North Anatolian Fault, is the semi-circular Turna Mountain west of Karliova. Both structures are composed of volcanic rocks having similar stratigraphic ages (Yılmaz *et al.* 1987; Şaroğlu & Yılmaz 1987; Şaroğlu & Yılmaz 1991). We can restore the position of the Turna Mountain opposite to the Bingöl half-caldera by a left-lateral displacement of 50 km along the mean direction of the North Anatolian and Main Varto Fault systems (Fig. 6b). As a result a volcano with a nearly conical morphology can be reconstructed. The caldera palaeo-topography along the North Anatolian Fault has been strongly modified by strike-slip faulting and related enhanced erosion. Secondary normal faulting affecting the Turna half-caldera (Fig. 6c) has also altered the initial volcanic structure. Despite the alterated original morphology, the reconstructed volcanic topography excludes any significant relative long-term vertical movement across the North Anatolian Fault. Indeed the topographic profile in Fig. 5c across the Turna/Bingöl volcano shows a

coherent triangular shape which center location is nearly identical to the center location of the Bingöl half caldera as defined by its summital shape.

The age of the volcanism around the Karliova Triple Junction is constrained by ^{40}Ar-^{39}Ar dating (Figs. 7, 8). ^{40}Ar-^{39}Ar ages were obtained on groundmass samples of lavas, with K concentrations ranging from 0.8% to 3.3%. As practically all terrestrial basalts, our samples show variable amounts of aqueous high- and low-temperature alteration, especially of the groundmass. Geologically meaningful results have been reported in spite of the alteration (e.g. Fleming *et al.* (1997) and references therein). In the present work we will show that consistent results can be obtained from whole rock samples by the deconvolution of the least altered Ar-bearing phases from the alteration products using the Ca-K and Cl-K ratios derived from Ar isotope systematic (see Villa *et al.* 2000). To unravel the effects of alteration, the most reliable criterion is a low Cl-K ratio, as Cl is observed to be characteristically high in secondary minerals. Steps having a constant and low Cl/K signature (which usually coincides with a constant and low Ca-K ratio, typical of groundmass) are termed "isochemical" and used to calculate a weighted average age. In two cases, no constant chemical ratios were obtained, but Cl-K ratios correlate with age, so that we performed a regression to zero chlorine (see Fig. 8).

The fact that lavas forming the Turna Mountains and the Bingöl half-caldera have similar ages (Figs. 7, 8) but distinct from the surrounding volcanism supports the morphological restoration of the caldera. The Turna Ar-Ar age of 2.85±0.05 Ma (sample Tu1 in Fig. 8c coherent with sample Tu2 in Fig. 8c and d) precisely matches the ages of the Bingöl half-caldera (samples Bi1: 3.13±0.09 Ma, Bi2: minimum age 3.11±0.33 Ma, Bi3: 3.1±0.29 Ma in Figs. 8a and b); these ages are coincident with, and are more reliable than, the whole-rock K-Ar ages obtained by Pearce *et al.* (1990) (see Fig. 7). Both half calderas rest on top of older volcanic rocks (Figs. 2, 7). The Turna volcanism lies on the 7.3 to 4.1 Ma old Solhan formation (see Fig. 7, and sample So1 in Fig. 8f). The age of this formation is quite well constrained near the East Anatolian Fault because its

volcanism was an obsidian source during prehistoric time (Chataigner *et al.* 1998; Poidevin 1998; Bigazzi *et al.* 1998). The Bingöl half-caldera lies to the north-west on the 6.9 to 5.6 Ma old volcanism of the Aras valley (Innocenti *et al.* 1982a) and to the north-east on the 8.3 to 6.0 Ma old Erzurum volcanism [8.3±0.1 Ma to 6.0±0.3 Ma (Innocenti *et al.* 1982a); 6.9±0.32 (Bigazzi *et al.* 1994); 6.83±0.36 (Bigazzi *et al.* 1997); 8.4±0.2 Ma (Chataigner *et al.* 1998)]. On the contrary the volcanism south of the Main Varto Fault is more recent than the Bingöl half-caldera as attested by fissure-fed lava flows and fault-related intrusions cross-cutting Bingöl related volcanic products (Buket & Görmüş 1986; Buket & Temel 1998). The latter is also supported by ^{40}Ar-^{39}Ar dating (Fig. 8) with samples taken at the base of and on the two main volcanic domes related to the Varto horsetail (Fig. 4). The ^{40}Ar-^{39}Ar ages (Fig. 8), although of lower precision, indicates that volcanism south of the Bingöl half caldera started 2.2±0.23 to 2.6±0.12 Ma ago (Fig. 8e) and that the two main volcanic domes are 0.46±0.24 Ma and 0.73±0.39 Ma old (Fig. 8g and h). Those ages are coherent with ages of fissure volcanisms further south along the Murat river across the Muş fold-and-thrust belt (Fig. 7; Bigazzi *et al.* 1996, 1998).

Finally the Bingöl/Turna lavas have an undistinguishable geochemistry considering major or trace elements, quite distinctive from the surrounding volcanism. In total alkali versus SiO_2 diagram (Fig. 9a) the Bingöl /Turna volcanic rocks form a well defined trend from basaltic trachy-andesite to the rhyolite field, and can be considered to be transitional between sub-alkaline and mildly alkaline in character. The more recent dyke volcanism just south of the Bingöl Half Caldera is mostly subalkaline but relative to the Bingöl /Turna one it has less alkali, is enriched in K-, Ni- and Sr- and depleted in Rb-. Furthermore Buket & Temel (1998) have clearly demonstrated that this volcanism is isotopically distinct from the Bingöl samples. The lavas just south of Turna Mountain, rich in obsidians (Catak-Alatepe sites of the Solhan formation) are rhyolites to be considered transitional between sub-alkaline and mildly alkaline trend. Compared to the Bingöl/Turna volcanism these lavas have more alkali, less Al_2O_3, less TiO_2, a high Rb/Sr ratio, high Ba- and low Zn-. Other volcanic rocks around

the East Anatolian Fault -Solhan Formation- are mostly basalts with a transitional character similar to the Bingöl/Turna volcanism but with less alkali, higher Mg-, Ti-, Ni- and Cr- content, lower Nb- and Zr-, and a very low Rb/Sr ratio.

Together with the fact that the two structures are truncated to the south and to the north by a continuous right-lateral fault system, all these observations strongly suggest that the Turna Mountain and the Bingöl half-caldera have a common origin, and are presently offset by about 50 km along the North Anatolian Fault.

Independently, one can also use the volcanism along the East Anatolian fault to further constrain its age and total offset. We estimate the total displacement of the East Anatolian fault by evaluating the offset of a metamorphic/Miocene body surrounded by volcanism (Fig. 2; Şaroğlu *et al.* 1992). A single structure can be reconstructed by a right-lateral displacement of 20±5km (Arpat & Şaroğlu 1972; Seymen & Aydın 1972; Şaroğlu *et al.* 1992; Westaway 1994, 2003). The Solhan volcanism just south of the so-reconstructed structure has similar age, and undistinguishable geochemistry across the East Anatolian Fault (samples represented with blue diamond in Figs. 7 and 9). In addition, the boundary of the single structure so obtained with the surrounding Solhan formation (6-4.1 Ma old) is smooth across the fault: this formation is not related to movement along the East Anatolian Fault and is clearly cross-cut by the later fault (Fig. 7). This shows that the age of the East Anatolian Fault should be less than 4 Ma as already proposed by others (e.g. Şaroğlu *et al.* 1992; Westaway & Aeger 2001). On the contrary, the lacustrine sediments and lignite deposits near Goynuk are most probably related to the extensional step-over of the East Anatolian Fault in that area (Fig. 7). The fact that those sediments are interbedded with the most recent volcanic products of the Turna Mountain suggests that the East Anatolian Fault was active in that area 2.88 Ma ago.

Evolution of the Anatolia-Eurasia-Arabia Triple Junction

The following scenario emerges. The complete Turna-Bingöl caldera was formed from 3.6 to 2.8 Ma ago, before being cut and right-laterally offset 50 km by the North Anatolian Fault. This offset is equal to (1) the Varto fault system total length and similar to (2) the geological offset of the North Anatolian Fault near Yedisu - offset of a thrust contact between ophiolitic mélange and volcanoclastic units (Herece & Akay 2003,appendix 13; Şengör *et al.* 2005)- and to (3) the offset of the Elmal-Periçay river system (Fig. 2)). Fissural volcanism related to the birth of the Varto fault system started 2.6 Ma ago. The volcano offset and volcanism age thus imply that the easternmost segment of the North Anatolian Fault and the present Triple Junction are younger than 2.8 Ma, establishing around 2.6 Ma ago. The deduced average slip rate of the North Anatolian Fault over the last 2.6 Ma of about 20 mm/yr roughly corresponds to its present-day rate. The later rate is however a lower bound as secondary deformation exists. With a complete formation of the East Anatolian Fault 2.8 to 3 Ma ago, we get a minimum geological slip rate of the East Anatolian Fault of 7 mm/yr, which is comparable to the 9-10 mm/yr GPS derived rate (McClusky *et al.* 2000; Reilinger *et al.* 2006) and to the 11 ± 1 mm/yr geomorphological rate determined further south (Çetin *et al.* 2003). The main puzzle remains the strong mismatch between the East Anatolian Fault ($\sim$3 Ma) and North Anatolian (12 Ma) ages that we discuss below.

It is well known that a two-phase extrusion process characterizes the India/Eurasia collision (Tapponnier *et al.* 1982). Westaway & Aeger (1996) suggest that a similar scenario is valid for the Anatolia extrusion, with a southward jump of the East Anatolian Fault. The North Anatolian Fault would have kept the same location because the stable Black Sea oceanic lithosphere prevents any new large fault propagation north of its present trace. The Anatolian extrusion would first occur between the North Anatolian Fault and a proto East Anatolian Fault, which can be identified with the left-lateral Ovacık-Malatya fault, located 110 km more to the west. An old Triple Junction would thus have been located in the Erzincan basin (Fig. 2). Our observations, and in particular the age difference between the

North Anatolian Fault (12 Ma), the East Anatolian Fault (2.8-3 Ma) and the present Triple Junction (2.6-2.8 Ma), strongly support this view. Our timing is however different from what Westaway (2004) proposes. The latest extrusion phase would have started about 2.6-3 Ma ago, with the activation of the East Anatolian Fault linked to the Dead Sea Fault and the jump of the Triple Junction to its present location near Karliova. This explains why the easternmost North Anatolian Fault must be younger than the North Anatolian segments west of Erzincan, and why the offset of the Bingöl Volcano is significantly smaller than the 85 km total offset of the North Anatolian Fault further west.

The eastward jump of the East Anatolian Fault may have different origins. It occurs at the same time as an increase in deformation and exhumation rates observed in many fold-and-thrust belts (e.g. Axen *et al.* 2001; Morton *et al.* 2003) within the collision zone. The latter has been interpreted as a large scale reorganization of the Arabia-Eurasia collision, 5±2 Ma ago (Allen *et al.* 2004). An other possible cause is the rapid post-3 Ma change in the Africa/Eurasia motion (Calais *et al.* 2003) directly affecting the Aegean subduction zone and thereby the kinematics of the Anatolian block (Fig. 1). A further possibility would be a direct connection with the arrival of the North Anatolian Fault into the Aegean 3 Ma ago (Gautier *et al.* 1999), which relaxed the elastic strain in the Anatolian lithosphere and transformed the North Anatolian Fault into a transform fault (Armijo *et al.* 2003; Flerit *et al.* 2004). A last cause might be the slab detachment that occurred beneath eastern Anatolia as discussed by Faccenca *et al.* (2006). Whatever its origin, this new set-up would make the extrusion process more efficient, consistently with the substantial increase of the slip rate of the North Anatolian Fault and the localization of deformation on the North Anatolian Fault present strand (Barka & Handcock 1984). Finally it coincides with the recent change in the kinematics in the area around the present intersection between the East Anatolian Fault and the Dead Sea fault (Yürür & Chorowicz 1998; Över *et al.* 2002, 2004).

We have tentatively modeled the overall evolution of Anatolia-Eurasia-Arabia Triple Junction using a plate-tectonic framework where deformation is associated with rigid block motion (Fig. 10). The kinematics of the Karliova and the old Erzincan Triple Junction is modeled as a Transform/Transform/Trench Triple Junction similar to the Mendocino Triple Junction (McKenzie & Morgan 1969). Approximating the behavior of the eastern Turkey continental lithosphere like an oceanic one though subject to caution may still be valid to the first order for the following reasons. First, Jimenez-Munt & Sabadini (2002) have shown that Anatolia had a hard lithospheric rheology. In addition, the eastern crust is only slightly thickened being on average less than 45 km thick so gravitational driving force may be neglected to the first order (Zor *et al.* 2003, Cakir & Erduran 2004). Finally, like oceanic lithosphere eastern Turkey has an anomalously thin (60 to 80 km) lithosphere (Angus *et al.* 2006), with an upper most mantle partly molten and asthenospheric material in close proximity to the base of the crust (Gök *et al.* 2003, Al-Lazki *et al.* 2003, Maggi & Priestley 2005).

Predictions from the above simple model are in good agreement with the observations. The length of the straight segment east of the Erzincan Triple Junction (segment 2 in Fig. 2; d_1+d_2 in Fig. 10d) do match the total offset of the North Anatolian Fault of 85 km. In addition a model of strain distribution (inset in Fig. 10c) resulting from motion along the "old" North Anatolian Fault (segments 1 and 2) and the "new" East Anatolian Fault is able to reproduce the non-trivial geometry of the new North Anatolian segments filling the gap between the Erzincan Triple Junction and the northern extremity of the East Anatolian Fault (segments 3 and 4 in Fig. 2; Fig. 10c). It is clearly seen in Fig. 10c that the relevant fault segments strikes coincide with the optimum failure planes for right-lateral faulting. A bilateral fault propagation is also favored due to strain increase centered at the extremities of the East Anatolian Fault and "old" North Anatolian segments. Moreover the 50 km offset of the Bingöl volcano, that records the offset of the North Anatolian Fault over the last 2.5 Ma, is equal to the offsets of the North Anatolian Fault near Yedisu and to the length of the

Varto fault corresponding to d_2 in Fig. 10d. Finally, the finite displacement vectors associated with the proposed kinematics over the last 2.5 Ma (Fig. 10f) are compatible with present-day motion on the North Anatolian Fault and East Anatolian Fault (McClusky *et al.* 2000; Reilinger *et al.* 2006) and with the predicted plate motion of Arabia relative to Eurasia at this location.

This proposed plate model is only a first estimate of the local kinematics. Our model particularly does not explain the apparent anti-clockwize rotation of 25° of the last 75 km long Karliova segment of the East Anatolian Fault with respect to the mean direction of the East Anatolian Fault further south as well as the related opening of the Bingöl Basin and related shortening which occurred to the north and north east of the Bingöl Basin. In addition our model does not account for secondary deformation that occurs within the plates away from the North Anatolian and East Anatolian Faults (Figs. 2-7; Jaffrey et al. 2004). For example near the Triple Junction secondary fault systems link the North Anatolian to the East Anatolian Fault. The latter deformation agrees with the first Triple Junction model of Westaway & Aeger (2001). In their model, when the right-lateral and left-lateral faults do not meet at a point like at the present Karliova Junction, a zone of distributed extension accommodates the deformation in between the strike-slip faults and the opening of the Karliova Basin. This situation may have prevailed just before the creation of the Karliova Triple Junction (Fig. 10c), and the observed normal faults and Karliova basin may be inherited from that time. Finally a unique trench system as modeled in Fig. 10 does not exist. The deformation is partitioned with mostly right-lateral deformation along the Main Varto Fault and shortening to the south along the Muş fold-and-thrust belt. Present active shortening is attested in the field by uplifted alluvial fans and thrust fault scarps. Recent seismicity does not show any thrusting events despite the dense coverage of the temporary seismic network (Örgülü *et al.* 2003), but the critical factor remains the short period of observation compared to the seismic cycle.

Finally to fully understand for the Triple Junction evolution one must account for the lithospheric complexities existing at the boundaries

between the Arabian, Eurasian and Anatolian blocks (Fig. 11). S-wave receiver functions (Angus et al. 2006) have shown that near the triple junction the signatures of at least three or four lithosphere-asthenosphere boundaries (LAB) can be found: the LAB of East Anatolian Accretionary Complex and Rhodope-Pontide continental fragment (called here "East Anatolian" LAB), the LAB of Anatolian Block (called here "Anatolian" LAB) and the LAB of the Arabian Shield (called here "Arabian" LAB). The Anatolian Faults and associated structures all have deep lithospheric signatures: along the North Anatolian Fault, an apparent lithospheric right-lateral offset corresponds to the Turna/Bingöl offset (see the isothickness line: 66 km in Fig.13); across the East Anatolian Fault until Bingöl Basin, a lithospheric step exists between the northern 70 km deep "East Anatolian" LAB, and the southern 80 km deep "Anatolian" and 115 km deep "Arabian" LAB. The Erzincan Basin, Bingöl Basin and Muş Basin are also deeply rooted: major lithospheric thinning is found in the Erzincan area, the location of the former triple junction; lithospheric thickening exists north and north west of the Bingöl Basin where shortening occurred due to the 25° change in strike of the East Anatolian Fault; the Bingöl Basin and Muş-basin-and-thrust-zone form at the junction between the "Arabian" LAB and the "East Anatolian" LAB, the Muş thrust zone being also limited to the north by a low velocity zone. A three dimensional mechanical model including fault discontinuity affecting the whole lithosphere is thus needed to understand in details the kinematics at the junction between Arabia, Anatolia and Eurasia.

Conclusion

The availability of a set of relevant data, together with the relative simplicity of the Anatolian fault system makes it a unique laboratory to study the long-term evolution of major strike-slip fault. Interestingly, the resulting picture is reminiscent of smaller scale faults or cracks evolution, as described in Hubert-Ferrari *et al.* (2003). The history of the North Anatolian Fault propagation is particularly rich and can be summarized as follows. From 12 Ma to 2.5 Ma, it has grown in length westward over 1300

km from Erzincan in eastern Turkey to the Aegan Sea with a slip rate of 3 mm/yr, and a propagation speed of 120 mm/yr (Armijo *et al.* 2003; Flerit *et al.* 2004). A similar propagation speed was computed for the Altyn Tagh fault, a main strike-slip fault in the extrusion system related to the India-Eurasia collision (Meyer *et al.* 1998; Metivier *et al.* 1998). Rift propagation can also have speed exceeding 100 mm/yr (e.g. Wilson & Hey 1995; Maniguetti *et al.* 1997), as well as the lateral propagation of the Himalaya front (Meigs *et al.* 1995; Husson *et al.* 2004). This propagation phenomenon is consistently associated with different ages of the fault (Şengör *et al.* 2005): ~ 12 Ma in the east (Şengör *et al.* 1985; Barka 1992), ~ 8.5 to 5 Ma in its central part (Hubert-Ferrari *et al.* 2002), ~ 5 Ma in the western Marmara sea (Straub *et al.* 1997; Armijo *et al.* 1999), ~ 3 Ma in the Aegean Sea (Gautier *et al.* 1999), ~ 1 Ma in the Gulf of Corinth at the westernmost end of the fault (Armijo *et al.* 1996). The most dramatic event in this long history is described in the present paper: 2.5 to 3 Ma ago, the slip rate along the North Anatolian Fault suddenly increases from about 3 mm/yr averaged in 10 Ma to about 20 mm/yr, at a time when part of the Arabian plate was accreted to Eurasia with the initiation of a new East Anatolian Fault. The Whakatane Graben (New Zealand) behaved in a similar way, fault growth was first characterized by tip propagation and relatively slow displacements, and then after fault linkage the average fault increased by almost threefold (Taylor *et al.* 2004).

Swiss National Science Foundation Grant, No. 21-65197.01 funded this work. The data bank of INSU-CNRS gave us access to the satellite imagery. Vincent Serneels (University of Fribourg, Switzerland) did XRF element analyses. Field work was successfully conducted with the help of Martin Burkhard and Altan Devrim. We thank Philippe Claeys for fruitful discussions. Reviews from Celal Şengör and another anonymous reviewer improved the manuscript.

Reference list

Allen, A., Jackson, J. & Walker. R. 2004. Late Cenozoic reorganization of the Arabia-Eurasia collision and the comparison of short-term and long-term deformation rates. *Tectonics*, **23**, TC2008, doi:10.1029/2003TC001530.

Al-Lazki, A.I., Seger, D., Sandvol, E., Turkelli, N., Mohamad, R. & Barazangi, M. 2003. Tomographic Pn velocity and anisotropy structure beneath the Anatolian plateau (eastern Turkey) and the sur rounding regions. *Geophysical Research Letter,* **30**, 8043, doi:10.1029/2003GL017391.

Altinli, E. 1961. *Geological map of Turkey*, *Erzurum Quadrangle*, General Directorate of Mineral Research and Exploration (eds.), Ankara.

Ambraseys, N.N. & Zatopek, A. 1968. The Varto Ustukran earthquake of 19 August 1966. *Bulletin of the Seismological Society of America*, **58**, 47-102.

Ambraseys, N. 1988. Engineering seismology. *Journal of Earthquake and Engeneering and Structural Dynamics*, **17**, 1-106.

Angus, D.A., Wilson, D.C., Sandvol, E. & Ni J.F. 2006. Lithospheric structure of the Arabian and Eurasian collision zone in eastern Turkey from S-wave receiver functions. *Geophysical Journal International*, **166**, 1335-1346 doi: 10.1111/j.1365-246X.2006.03070.x.

Armijo, R., Meyer, B., King, G.C.P., Rigo, A. & Papanastassiou, D. 1996. Quaternary evolution of the Corinth rift and its implications. *Geophysical Journal International*, **126**, 11-53.

Armijo, R., Meyer, B., Hubert-Ferrari, A. & Barka, A. A. 1999. Propagation of the North Anatolian Fault into the Northern Aegean: Timing and Kinematics. *Geology*, **27**, 267-270.

Armijo, R., Flerit, F., King, G.C.P. & Meyer, B. 2003. Linear elastic fracture mechanics explains the past and present evolution of the Aegean. *Earth and Planetary Science Letters*, **217**, 85-95.

Arpat, E. & Şaroğlu, F. 1972. The East Anatolian Fault system: thoughts on its development. *General Directorate of Mineral research and Exploration (MTA) Bulletin*, **78**, 33-39.

Axen, G.J., Lam, P.S., Grove, M., Stockli, D.F. & Hassanzadeh, J. 2001. Exhumation of the west-central Alborz Mountains, Iran, Caspian subsidence, and collision-related tectonics. *Geology*, **29**, 559-562.

Barka, A.A., & Hancock, P.L. 1984. Neotectonic deformation patterns in the convex-northwards arc of the North Anatolian fault. In: Dixon, J.G. & Robertson, A.H.F *The Geological Evolution of the eastern Mediterranean*. Geological Society, London, Special Publication, **17**, 763-773.

Barka, A & Kadinsky-Cade, K. 1988. Strike-slip fault geometry in Turkey and its influence on earthquake activity. *Tectonics*, **7**, 663-684

Barka, A.A. & Gülen, L. 1989. Complex evolution of the Erzincan basin (eastern Turkey). *Journal of Structural Geology*, **11**, 275-283.

Barka, A.A. 1992. The North Anatolian fault zone. *Annales Tectonicae (Suppl.)*, **6**, 164-195.

Bigazzi, G., Yeginğil, Z., Ercan, T., Oddone, M. & Ozdoğan, M. 1994. Provenance studies of prehistoric artefacts in Eastern Anatolia: first results of an interdisciplinary research. *Mineralogica et Petrographica Acta*, **XXXVII**, 17-36.

Bigazzi, G., Yeginğil, Z., Ercan, T., Oddone, M. & Ozdoğan M. 1996. The Pisa-Adana joint project of prehistoric obsidian artifacts; first results from eastern Anatolia using fission track dating method: an overview. *In*: Dimirci, S. Över A.M. & Summers, G.D. (eds) *Proceedings of the 29th symposium on Archaeometry, Ankara, 9-14 May 1994.* Archaeometry, Tübitak, Ankara, **94**, 521-528.

Bigazzi, G., Yegingil, Z., Ercan, T., Oddone, M., Ozdogan, M. 1997. Age determination of obsidian bearing volcanic s in Eastern Anatolia using the fission track dating method. *Geological Bulletin of Turkey*, **40**, 57-72.

Bigazzi, G., Poupeau, G., Yeginğil, Z. & Bellot-Gurlet, L. 1998. Provenance studies of obsidian artefacts in Anatolia using the fission track dating

method. An overview. *In:* Gourgaud, A., Gratuze, B., Poupeau, G., Poidevin, J.L.& Cauvin, M.C. (eds) *L'Obsidienne au Proche et Moyen Orient, du Volcan à l'Outil*. BAR International Series Hadrian Books (Oxford) **738**, 69-89.

Bingöl, E., Bal, I. & Can, N. 1989. *Geological map of Turkey*, scale 1: 2000 000, MTA- General Directorates of Mineral Research and Exploration (eds.), Ankara, Turkey.

Bozkurt, E., & Koçyiğit, A., 1996. The Kazova Basin: an active flower structure on the Almus Fault Zone, a splay fault system of the North Anatolian Fault Zone, Turkey. *Tectonophysics,* **265**, 239-254.

Bozkurt, E., 2001. Neotectonics of Turkey-a synthesis. *Geodinamica Acta*, **14**, 3-30.

Buket, E. & Görmüş, S. 1986. Varto (Muş) havzasındaki Tersiyer yaşlı istifin stratigrafisi. *Yerbilimleri* **13**, 17-29, (in Turkish with English abstract).

Buket, E. & Temel, A. 1998. Major-element, trace element, and Sr-Nd isotopic geochemistry and genesis of Varto (Muş) volcanic rocks, Eastern Turkey. *Journal of Volcanology and Geothermal Research*, **85**, 405-422.

Çakir, Ö. & Erduran, M. 2004. Constraining crustal and uppermost mantle structure beneath station TBZ (Trabzon, Turkey) by receiver function and dispersion analyses. Geophysical Journal International, **158**, 955-971.

Calais, E., DeMets, C. & Nocquet, J.-M. 2003. Evidence for a post-3.16-Ma change in Nubia-Eurasia-North America plate motions ? *Earth and Planetary Science Letters*, **216**, 81-92.

Çetin, H., Güneyli, H. & Mayer, L. 2003. Paleoseismology of the Palu-Lake Hazar segment of the East Anatolian Fault Zone, Turkey. *Tectonophysics*, **374**, 163-197.

Chataigner, C., Poidevin, J.L. & Arnaud, N.O. 1998. Turkish occurrences of obsidian and use by prehistoric peoples in the Near East from 14,000 to 6000 BP. *Journal of Volcanology and Geothermal Research*, **85**, 517-537.

Dewey, J.F., Hempton, M.R., Kidd, W.S.F., Şaroğlu, F. & Şengör, A.M.C. 1986. Shortening of continental lithosphere: the neotectonics of eastern Anatolia-A young collision Zone. *In:* Coward, M.P. & Ries, A.C. (eds.) *Collision Tectonics*. Geological Society of London, Special Publication, **19,**3-36.

Faccenna, C., Bellier, O., Martinod, J., Piromallo, C. & Regard, V. 2006, Slab detachment beneath eastern Anatolia. *Earth and Planetary Science Letters*, **242**, 85-97.

Fleming, TH., Heimann, A., Foland, KA., & Elliot, DH. 1997. Ar-40/Ar-39 geochronology of Ferrar Dolerite sills from the Transantarctic mountains, Antarctica: Implications for the age and origin of the Ferrar magmatic province. *Geological Society of America Bulletin,* **109**, 533-546.

Flerit, F., Armijo, A., King, G., & Meyer, B. 2004. The mechanical interaction between the propagating North Anatolian Fault and the back-arc extension in the Aegean. *Earth and Planetary Science Letters*, **224**, 347-362.

Fuenzelida, H., Dorbath, L., Cisternas, A., Rivera, L., Eyidoğan, H., Barka, A.A., Haessler, H., Philip, H. & Lybéris, N. 1997. Mechanism of the Erzincan earthquake and its aftershocks, tectonics of the Erzincan basin and decoupling on the North Anatolian Fault. *Geophysical Journal International*, **129**, 1-28.

Gautier, P., Brun, J.-P., Richard, M., Dimitrios, S., Martinod, J. & Jolivet, L. 1999. Timing, kinematics and cause of Aegean extension: a scenario based on a comparison with simple analogue experiments. *Tectonophysics*, **315**, 31-72

Gelati, R. 1975. Miocene marine sequence from lake Van eastern Turkey. *Rivista Italiana di Paleontologia e stratigraphia*, **81**, 477-490.

Gök, R., Sandvol, E., Tükelli, N., Seber, D., & Barazangi, M. 2003. Sn attenuation in the Anatolian and Iranian plateau and surrounding regions. *Geophysical Research Letter,* **30**, 8042,

doi:10.1029/2003GL018020.

Gürsoy, H., Piper, J.D.A., Tatar, O. & Temiz, H. 1997. A palaeomagnetic study of the Sivas basin, Central Turkey: Crustal deformation during lateral extrusion of the Anatolian block. *Tectonophysics*, **271**, 89-105.

Herece, E. & Akay, E. 2003. Kyzey Anadolu Fayi (KAF) Atlasi/ Atlas of North Anatolian Fault (NAF). Maden Tetk. Arama Genl Müdürlügü, Özel Yayın. Ser. 2, Ankara, [IV], 61 pp. + 13 appendices as separate maps.

Hubert-Ferrari, A., Armijo, R., King, G.C.P., Meyer, B. & Barka, A. 2002. Morphology, displacement and slip rates along the North Anatolian Fault (Turkey). *Journal of Geophysical Research*, **107**, 10,1029-10,1059.

Hubert-Ferrari, A., King, G.C.P., Manighetti, I., Armijo, R., Meyer, B. & Tapponnier, P. 2003. Long-term Elasticity in the Continental Lithosphere; Modelling the Aden Ridge Propagation and the Anatolian Extrusion Process. *Geophysical Journal International*, **153**, 111-132.

Husson, L., Mugnier, J-L., Leturmy, P. & Vidal, G. 2004. Kinematics and sedimentary balance of the Subhimalayan range, W. Nepal. *In:* MacClay, K. (ed), *Thrust Tectonics and Hydrocarbon Systems*. AAPG Memoir, **82**, 115-130.

Innocenti, F., Mazzuoli, R., Pasquare, G., Radicati di Brozol, F. & Villari L. 1982a. Tertiary and Quaternary volcanism of the Erzurum-Kars area Eastern Turkey: geochronological data and geodynamic evolution. *Journal of Volcanology and Geothermal Research*, **13**, 223-240.

Innocenti, F., Manetti, P., Mazzuoli, R., Pasquare, G. & Villari, L. 1982b. Anatolia and North-western Iran. *In:*. Thorpe, R.S (ed) *Andesites; orogenic andesites and related rocks*. John Wiley and Sons, 327-349.

Jaffey, N., Robertson, A. & Pringle, M. 2004. Latest Miocene and Pleistocene ages of faulting, determined by ^{40}Ar-^{39}Ar single-crystal dating of air fall tuff and silicic extrusives of the Erciyes Basin, central Turkey: evidence for intraplate deformation related to the

tectonic escape of Anatolia. *Terra Nova,* **16,** 45-53.

Jimenez-Munt, I., & Sabadini, R. 2002. The block-like behavior of Anatolia envisaged in the modeled and geodetic strain rates. *Geophysical Research letter,* **29**, doi: 10.1029/2002GL015995, 2002.

Kim, Y.-S. & Sanderson, D.J 2006. Structural similarity and variety at the tips in a wide range of strike-slip faults: a review. *Terra Nova*, **18**, 330-344 , doi: 10.1111/j.1365-3121.2006.00697.x.

Manighetti, I., Tapponnier, P., Courtillot, V., Gruszow, S. & Gillot, P. 1997. Propagation of rifting along the Arabia-Somalia plate boundary: the Gulfs of Aden and Tadjoura. *Journal of Geophysical Research*, **102**, 2681-2710.

Maggi, A. & Priestley, K. 2005. Surface waveform tomography of the Turkish-Iranian plateau. *Geophysical Journal International,* **160**, 1068-1080.

McClusky, S., Balassanian, S., Barka, A., Demir, C., Ergintav, S., Georgiev, I., Gurkan, O., Hamburger, M., Hurst, K., Kahle, H., Kastens, K., Kekelidze, G., King, R., Kotzev, V., Lenk, O., Mahmoud, S., Mishin, A., Nadariya, M., Ouzounis, A., Paradissis, D., Peter, Y., Prilepin, M., Reilinger, R., Sanlı, I., Seeger, H., Tealeb, A., Toksöz, M. N., & Veis, G. 2000. GPS constraints on plate motion and deformation in the eastern Mediteranean: Implication for plate dynamics. *Journal of Geophysical Research*, **105**, 5695-5719.

McKenzie, D.P. & Morgan, W.J. 1969. Evolution of triple junctions. *Nature*, **224**, 125-133.

McKenzie, D.P., 1972. Active tectonics of the Mediterranean region. *Geophysical Journal of the Royal Astronomical Society*, **30**, 109-185.

McQuarrie, N., Stock, J.M., Verdel, C. & Wernicke, B.P. 2003. Cenozoic ecolution of neotethys and implications for the causes of plate motions. *Geophysical Research Letters,* **30**, 2036, doi:10.1029/2003GL017992.

Meigs, A. J., Burbank, D. W. & Beck, R. A., 1995. Middle-late Miocene (>10 Ma) formation of the Main Boundary Thrust in the western Himalaya. *Geology*, **23**, 423-426.

Métivier, F., Gaudemer, Y., Tapponnier, P. & Meyer, B. 1998. Northeastward growth of the Tibet plateau deduced from balanced reconstruction of two depositional areas: The Qaidam and Hexi Corridor basins, China. *Tectonics*, **17**, 823-842.

Meyer, B., Tapponnier, P., Bourjot, L., Metivier, F., Gaudemer, Y., Peltzer, G., Shunmin, G. & Zhitai, C., 1998. Crustal thickening in Gansu-Qinghai, lithospheric mantle subduction and oblique, strike-slip controlled growth of the Tibetan Plateau. *Geophysical Journal International*, **135**, 1-47.

Morton, A., Allen, M., Simmons, M., Spathopoulos, F., Still, J., Hinds, D., Ismail-Zadeh, A. & Kroonenberg, S. B. 2003. Provenance patterns in a neotectonic basin: Pliocene and Quaternary sediment supply to the South Caspian. *Basin Research,* **15**, 321-337.

Örgülü, G., Aktar, M., Türkelli, N., Sandvol, E. & Barazangi, M. 2003. Contribution to the seismotectonics of Eastern Turkey from moderate and small size events. *Geophysical Research Letters,* **30**, 8040.

Över, S., Ozden, S. & Unlugenc, U.C. 2004. Late Cenozoic stress distribution along the Misis Range in the Anatolian, Arabian, and African Plate intersection region, SE Turkey. *Tectonics*, **23,** TC3008, doi:10.1029/2002TC001455.

Över, S., Unlugenc, U.C., & Bellier, O. 2002. Quaternary stress regime change in the Hatay region (southeastern Turkey). *Geophysical Journal International*, **148**, 649-662.

Pearce, J. A., Bender, J.F., De Long, S. E., Kidd William, S.F., Low, P.J., Güner, Y., Şaroğlu, F., Yılmaz, Y., Moorbath, S. & Mitchell, J.G. 1990. Genesis of collision volcanism in eastern Anatolia, Turkey. *Journal of Volcanology and Geothermal Research*, **44**, 189-229.

Poidevin J.L., 1998. Provenance studies of obsidian artefacts in Anatolia using the fission track dating method. An overview. *In:* Gourgaud, A., Gratuze, B., Poupeau, G., Poidevin, J.L.& Cauvin, M.C. (eds)

L'Obsidienne au Proche et Moyen Orient, du Volcan à l'Outil. BAR International Series Hadrian Books (Oxford) **738**, 105-156.

Reilinger, R., McClusky, S., Vernant, P., Lawrence, S., Ergintav, S., Cakmak, R., Ozener, H., Kadirov, F., Guliev, I., Stepanyan, R., Nadariya, M., Hahubia, G., Mahmoud, S., Sakr, K., ArRajehi, A., Paradissis, D., Al-Aydrus, A., Prilepin, M., Guseva, T., Evren, E., Dmitrotsa, A., Filikov, S.V., Gomez, F., Al-Ghazzi R. & Karam G. 2006. GPS constraints on continental deformation in the Africa-Arabia-Eurasia continental collision zone and implications for the dynamics of plate interactions. *Journal Geophysical Research*, **111**, B05411, doi:10.1029/2005JB004051.

Şaroğlu, F. & Yılmaz, Y. 1987. Geological evolution and basin models during neotectonic episode in the eastern Anatolia. *Bulletin Mineral Research and Exploration*, **107**, 61-83.

Şaroğlu, F. & Yılmaz Y. 1991. Geology of the Karliova region: intersection of the North Anatolian and East Anatolian Transform Faults. *Bulletin of the Technical University of Istanbul*, **44**, 475-493.

Şaroğlu, F., Emre, Ö. & Kuşçu, I. 1992. The east Anatolian fault zone of Turkey. *Annales Tectonicae, Special Issue*, **6**, 99-125.

Şengör, A.M.C., Görür, N. & Şaroğlu F. 1985. Strike-slip faulting and related basin formation in zones of tectonic escape: Turkey as a case study. *In:* Biddle, K.T. & Christie-Blick, N. (eds) *Strike-slip faulting and Basin formation*. Society of Economic Paleontologists and Mineralogist, Special Publication, 227-267.

Şengör, A.M.C., Tüysüz, O., İmren, C., Sakınç, M., Eyidoğan, H., Görür, N., Le Pichon, X. & Rangin, C. 2005. The North Anatolian Fault: A new look. *Annual Review of Earth and Planetary Science*, **33**, 1-75.

Seymen, İ. & Aydın, A. 1972. The Bingöl earthquake fault and its relation to the North Anatolian Fault Zone. *General Directorate of Mineral research and Exploration (MTA) Bulletin,* **79**, 1-8 (in Turkish with English abstract).

Straub, C., Khale, H.G. & Schindler C., 1997. GPS and geological estimates of the tectonic activity in the Marmara Sea region, NW Anatolia. *Journal Geophysical Research*, **102**, 27,587-27,601.

Tapponnier, P. 1977. Evolution tetonique du systeme alpin en Mediterranee: Poinconement et ecrasement rigide-plastique, *Bulletin de la Soci□ G□logique de France* , **7**, 437-460.

Tapponnier, P., Peltzer G., Le Dain A. Y., Armijo R. & Cobbold, P., 1982. Propagating extrusion tectonics in Asia: new insights from simple experiments with plasticine. *Geology*, **10**, 611-616.

Tarhan, N. 1993. *Geological Map of the Erzurum*. General Directorate of Mineral Research and Exploration, Ankara, **G32 Quadrangle**.

Tarhan, N. 1994. *Geological Map of the Erzurum*. General Directorate of Mineral Research and Exploration, Ankara, **G31 Quadrangle**.

Tatar, O., Piper, J.D.A., Gürsoy, H. & Temiz, H., 1996. Regional significance of neotectonic anticlockwise rotation in central Turkey. *International Geology Review,* **38**, 692-700.

Taylor, S.K., Bull, J.M., Lamarche, G. & Barnes, P.M. 2004. Normal fault growth and linkage in the Whakatane Graben, New Zealand, during the last 1.3 Myr. *Journal of Geophysical Research*, **109,** B02408, doi:10.1029/2003JB002412.

Villa, I.M., Hermann, J., Müntener, O. & Trommsdorff, V. 2000. ^{39}Ar-^{40}Ar dating of multiply zoned amphibole generations (Malenco, Italian Alps). *Contributions to Mineralogy and Petrology*, **140**, 363-381.

Wallace, R.E. 1968. Earthquake of august 19, 1966. Varto Area, Eastern Turkey. *Bulletin of the Seismological Society of America*, **58**, 11-45.

Westaway, R. 1994. Present-day kinematics of the Middle East and eastern Mediterranean. *Journal of Geophysical Research*, **99**, 12071-12090.

Westaway, R. & Aeger, J., 1996. The Gölbasi basin, Southern Turkey: a complex discontinuity in a major strike-slip fault zone. *Journal Geological Society of London*, **153**, 729-744.

Westaway, R. & Aeger, J. 2001. The kinematics of the Malatya-Ovacik Fault zone. *Geodinamica Acta*, **14**, 103-131.

Westaway, R., 2003. Kinematics of the Middle East and Eastern Mediterranean Updated. *Turkish Journal of Earth Sciences*, **12**, 5-46.

Westaway, R., 2004. Kinematic consistency between the Dead Sea Fault

Zone and the Neogene and Quaternary left-lateral faulting in SE Turkey. *Tectonophysiscs*, **391**, 203-237.

Wilson, D.S. & Hey, R.N. 1995. History of rift propagation and magnetization intensity for the Cocos-Nazca spreading center. *Journal of Geophysical Research*, **100**, 10041-10056.

Yılmaz, Y., Şaroğlu, F. & Güner, Y. 1987. Initiation of the neomagmatism in East Anatolia. *Tectonophysics*, **134**, 177-199.

Yürür, M. T. & Chorowicz, J., 1998. Recent volcanism, tectonics and plate kinematics near the junction of the African, Arabian and Anatolian plates in the eastern Mediterranean. *Journal of Volcanology and Geothermal Research*, **85**, 1-15.

Zor, E., Sandvol, E., Gürbüz, C., Türkelli, N., Seber, D. & Barazangi, M. 2003. The crustal structure of the East Anatolian plateau (Turkey) from receiver functions. Geophysical Research Letter, **30**, 8044, doi:10.1029/2003GL018192.

FIGURE CAPTION

Figure 1: Continental extrusion of the Anatolian block away from the Arabia-Eurasia collision zone. The current GPS vectors relative to Eurasia are indicated (McClusky *et al.* 2000). NAF: North Anatolian Fault, EAF: East Anatolian Fault, DSF: Dead Sea Fault, ASZ: Aegean Subduction Zone. Box is area of Figure 2.

Figure 2: The Anatolia/Eurasia/Arabia Triple Junction: present fault geometry, seismicity (focal mechanisms and earthquake ruptures), volcanism and sedimentary basins (see location in Figure 3). Boxes are areas of Figures 3, 4, 5, 6. Total offset on the East Anatolian Fault (EAF) constrained by 20±5 km offset of a metamorphic body bounded by Miocene sediments and volcanism (Şaroğlu *et al.* 1992).

Figure 3: Right-laterally offset morphology along easternmost segment of the North Anatolian Fault (see location in Figure 2). Top: Spot image.

Bottom: Interpretation confirmed by fieldwork, showing river offsets reaching 3.7 km, and river captures (offsets d and e).

Figure 4: Deformation splaying east of Karliova Triple Junction forming the large Varto horsetail (see location in Figure 2). Main Varto Fault at the foot of the Bingöl Caldera accommodates mainly right-lateral deformation with a thrusting component at its eastern extremity. Secondary right-lateral and normal deformation associated with volcanic domes occurs to south. Top: Spot image. Bottom: Interpretation confirmed by fieldwork. Inset: beheaded drainage system along the Main Varto fault confirming right-lateral motion.

Figure 5: Photos of the volcanic domes associated with the Varto Fault system (viewpoints in Figure 4).

Figure 6: Volcano reconstruction by a 50 km left-lateral displacement along North Anatolian and Main Varto Fault systems (see location in Figure 2).
a. Present morphology of the junction of the North and East Anatolian Faults with active faults in black and volcanism. Thick lines: main faults; thin lines: secondary faults; lines with ticks: normal motion component.
b. After restoration of 50 km, the Turna and Bingöl mountains are put in front of each other, reconstructing a single volcanic edifice. Volcano palaeo-topography is strongly modified along the North Anatolian and Main Varto Fault systems. On its southeast flank, normal faulting also deforms the topography. The somital shape of the Bingöl half-caldera has an elliptical shape reflecting a slight elongation of the volcano in a Northwest-Southeast direction.
c. Topographic profile across the restored volcano. The location of volcano center extrapolating upward the volcano flanks is nearly identical to the one derived from the somital shape of the Bingöl half caldera showing that long-term uplift across the North Anatolian Fault is negligible.

Figure 7: Detail mapping of volcanism at the triple junction with location of volcanic samples and ages (see location in Figure 2, and age spectra in

Figure 8). Mapping of the Turna and Bingöl volcanism done combining fieldwork, Landsat images, and reinterpreted published geological maps (Altinli 1961; Bingöl *et al.* 1989; Tarhan 1993, 1994; Buket & Temel 1998; Herece & Akay 2003). Locations of samples of Pearce *et al.* (1990), Buket & Temel (1998), Poitevin (1998) used in Fig. 9 are shown. Samples from Bingöl Mt. (Bi1: 3.1±0.09 Ma; Bi2: min. age 3.1 Ma; Bi3: 3.1±0.3 Ma) and Turna Mt. (Tu1: 2.88±0.06 Ma; Tu 2: 2.3-3.9Ma) show similar ^{40}Ar-^{39}Ar ages, while Sohlan volcanism south of Turna Mt. (So1: 5.39±0.12 Ma) is older and fissural Varto volcanism is younger (Va1 and Va2 sampled at the base of the domes along incised river valley have ages of 2.6±0.12, 2.2±0.23 Ma respectively, whereas Va3 and Va4 sampled on the flank of the domes have ages of 0.46±0.24Ma and 0.73±0.4 Ma respectively). Ages obtained are coherent with other published ^{40}Ar-^{39}Ar, K-Ar, and fission track ages.

Figure 8: ^{40}Ar-^{39}Ar dating age spectra for lavas near the triple junction (see sample locations in Figure 7). Analytical procedures of the stepwize heating exactly followed the ones detailed in Villa *et al.* (2000).

a. Age spectrum for sample Bi1, Bi2, Bi3; Bi1 isochemical age is 3.13 ± 0.09 Ma (1 sigma error) using steps 5-7 having Cl-K ratio< 0.0046; Bi2 zero Cl minimum age is 3.11 ±0.33 Ma; for Bi3, steps 3 and 4, having Cl-K ratio< 0.0052 and Ca-K ratio< 3, define an isochemical age of 3.11 ± 0.29 Ma.

b. Three-isotope correlation plot for Bi2; the zero-Cl minimum age is 3.11 ± 0.33 Ma using a regression on steps 1-5.

c. Age spectrum for sample TU1 and TU2; TU1 isochemical age is 2.88 ± 0.06 Ma using step 4-7 having Cl-K ratio< 0.00015.

d. Three-isotope correlation plot for TU1 and TU2. The usual criteria (low Cl-K and Ca-K ratios) produce no simple pattern for TU2. Steps 3-6 with relatively low Cl-K ratio have ages in the range 2.3-3.9 Ma. Comparison with less altered TU1, and with other more altered samples of the North Anatolian Fault suite, suggests that two distinct alteration episodes are recorded, both revealed by high Cl-K ratios. Zero-Cl extrapolations of the two trends are compatible with the 2.85 Ma age of TU1.

e. Age spectrum for samples Va1 and Va2. For Va2, the Ca-K ratios are

bimodally distributed and require two phases; the isochemical age, calculated on the K-rich steps 1-4, is 2.22 ± 0.23 Ma. For Va1, the isochemical age on steps 1-6, having Cl-K ratio< 0.008, is 2.60 ± 0.12 Ma.
f. Age spectrum for sample SO1. The isochemical age is 5.39 ± 0.12 Ma on steps 2-7.
g. Age spectrum for samples Va3 and Va4. The Va4 isochemical age is 0.73 ± 0.39 Ma on steps 1-4.
h. Three-isotope correlation plot for sample Va3. The zero-Ca regression age is 0.46 ± 0.24 Ma using steps 2-5. Both Va3 and Va4 samples robustly define an age < 1 Ma for the latest phase of Varto fissural volcanism south of Bingöl half-caldera.

Figure 9: Plot of some major, minor and trace elements for samples located in figure 7. Data show that the Bingöl and Turna volcanisms (red dash line group) are similar, whereas the volcanisms south of the Bingöl half-caldera and along the East Anatolian Fault have different characteristics. Volcanism south of the metamorphic body mapped in Fig.7 on either side of the East Anatolian Fault is identical (blue dashed line group) confirming a total offset of 20± 5 km on the East Anatolian Fault and an activation of the East Anatolian Fault after the deposition of the Solhan volcanism that ends 4.4 Ma ago. Varto Fissural volcanism (dark dashed line group) has slightly evolved (see black arrow) through time. Dark filled triangles represent lavas at the base of the fissural volcanism, open triangles lavas of the domes, and black crosses volcanism at the eastern end of the Varto fault system.

Figure 10: Possible evolution of the Anatolia/Eurasia/Arabia Triple Junction assuming that faults separate rigid blocks.
a. Birth of a triple junction (TJ) in an extrusive plate system where a main left-lateral strike-slip fault meets a main right-lateral strike-slip fault like the North Anatolian Fault. Triple Junction corresponds to Erzincan triple junction.

b. Geometry of Transform/Transform/Trench Triple Junction after a North Anatolian Fault total slip of *d*. Triple Junction moves westward at slip rate of the North Anatolian Fault (McKenzie and Morgan, 1969). Eurasia/Arabia boundary accommodates both right-lateral and reverse motion and has a length equal to total slip *d* of the North Anatolian Fault. Triple Junction is stable because the North Anatolian Fault and the Eurasia/Arabia boundary are collinear.

c. Propagation of new left-lateral strike-slip fault (EAF) into Arabia at a time when $d=d_1$. At eastern extremity of the North Anatolian Fault (NAF) new fault segments are created as a link with East Anatolian Fault and a new triple junction (Karliova TJ) is activated. By this process part of the Arabian plate is accreted to the Anatolian plate. Inset: stress field and optimal failure planes around the North and East Anatolian tips at a time just before establishment of present easternmost North Anatolian segments and creation of Karliova Triple Junction. Gray segments are deep seated localized shear zones representing the North and East Anatolian Faults with a geometry similar to Fig. 9c. Optimal right-lateral failure planes for right lateral faulting (white segments) have orientations similar to North Anatolian Fault observed fault geometry west to the present Triple Junction (segments 3 and 4 in 10e represented by bold black segments).

d. Geometry after a total slip of $d=d_1 + d_2$ on North Anatolian Fault. Karliova Triple Junction kinematics is identical to Fig. 10a, and in particular the total length of the new Eurasia/Arabia plate boundary (d_2) is equal to North Anatolian Fault offset over the last 2.5 Ma.

e. Present fault geometry to compare to plate model in d). Structural elements like in Fig. 2.

f. Triangular vector diagram constrained by strikes of North and East Anatolian Faults, and by slip rates and finite displacement along both faults. Slip rate along the Varto-Muş fault system may be inferred in this way. Gray arrow represents velocity of Karliova derived from an Eulerian vector for Arabia/Eurasia (23.5°N, 23.8°E, 0.5° /Ma) within the errors bounds of the McClusky *et al.* (2000) pole (25.6±2.1°N, 19.7±4.1°E, 0.5±0.1°/Ma).

Figure 11: Lithospheric complexities at the Anatolia/Eurasia/Arabia triple junction. Lithosphere-asthenosphere boundary maps obtained from S-wave receiver functions (Angus *et al.* 2006) superposed on fault map and volcanism as in Fig. 2. The North and East Anatolian Faults, and associated structures appear to be rooted deeply in the lithosphere.

Note that the 75 km long Karliova segment of the East Anatolian Fault scales exactly with the lithospheric thickness and seems rotated anti-clockwize by 25 degree with respect to the mean strike of the East Anatolian Fault further south.

Figure 1

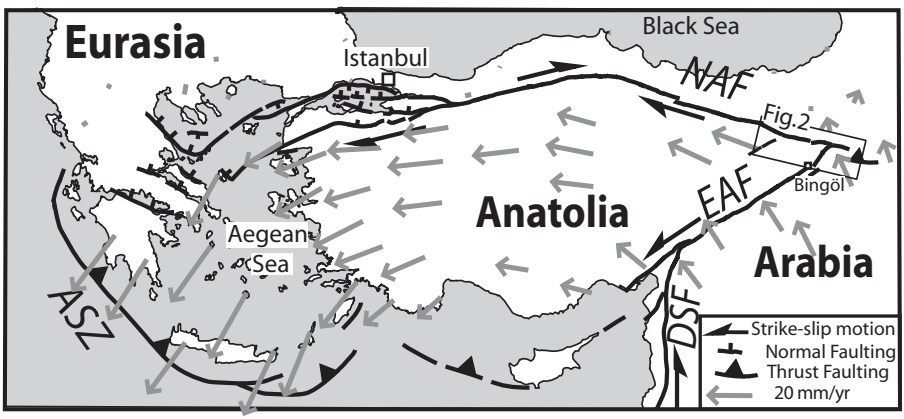
Eurasia
Black Sea
Istanbul
NAF
Fig.2
Bingöl
EAF
Anatolia
Arabia
Aegean
Sea
ASZ
DSF
Strike-slip motion
Normal Faulting
Thrust Faulting
20 mm/yr

Figure 2

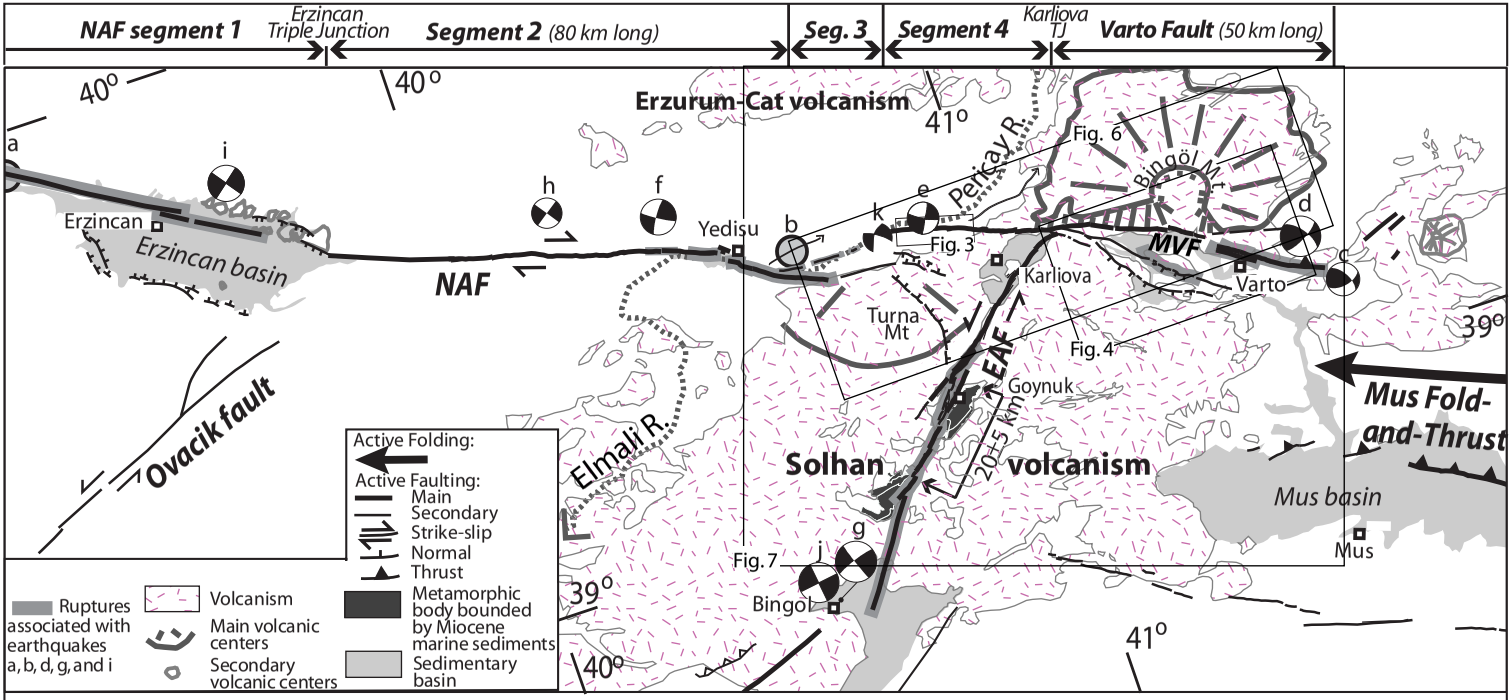

NAF, North Anatolian fault; **EAF,** East Anatolian Fault; **MVF**, Main Varto Fault. Major earthquakes: **a**, 26/12/39, Ms=7.9 (McKenzie, 1972); **b**, 17/08/49, Ms=7, (Ambraseys, 1988); Ms=5.6 (McKenzie, 1972); **d,** 19/08/66 (McKenzie, 1972); **e,** 20/08/66, Ms=5.3 (McKenzie, 1972); **f,** 26/07/67, Ms=6.0 (McKenzie, 1972); **g,** 22/05/71, Ms=6.9, (Taymaz et al., 1991); **h,** 20/05/89, Ms=5.1 (CMT, Harvard); **i,** 13/03/92, Ms=6.9 (Fuenzelida et al., 1997); **j**, 1/05/03, Ms=6.4 (Orgulu et al., 2003); **k**, 12/03/05, Mw=5.6, 14/03/05, Mw=5.8, 23/03/05, Mw=5.6 (CMT, Harvard).

Figure 3

Perıçay River
2000m
2250m
2500m
2750m
0.7-1.35 km
0.7-1.1 km
1.1-1.35 km
1.35 km
1.35 km
1.35-1.75 km
3.7 km
1.35 km
2.5 km
N
NAF fault trace
River
Present alluvium
Recent alluvium
Older alluvium
right-lateral offsets of the drainage system and associated alluvium
2750m
2500 m
2250 m
2000 m
Elevation

Figure 4

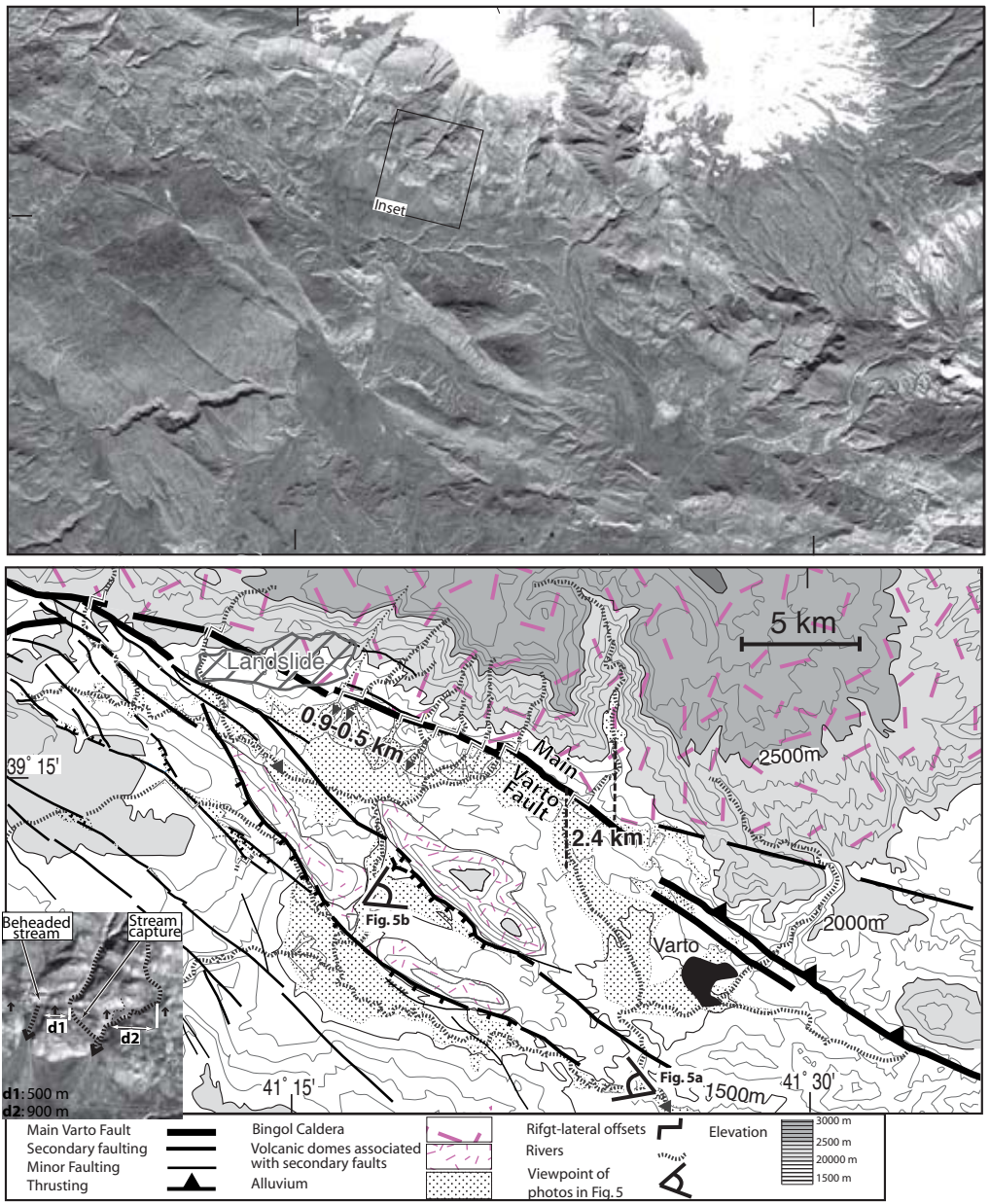
Inset
5 km
Landslide
0.9-0.5 km
Main
Varto
Fault
2.4 km
2500m
2000m
1500m
39° 15'
41° 15'
41° 30'
Fig. 5b
Fig. 5a
Varto
Beheaded stream
Stream capture
d1
d2
d1: 500 m
d2: 900 m
Main Varto Fault
Secondary faulting
Minor Faulting
Thrusting
Bingol Caldera
Volcanic domes associated with secondary faults
Alluvium
Rifgt-lateral offsets
Rivers
Viewpoint of photos in Fig. 5
Elevation
3000 m
2500 m
20000 m
1500 m

Figure 5

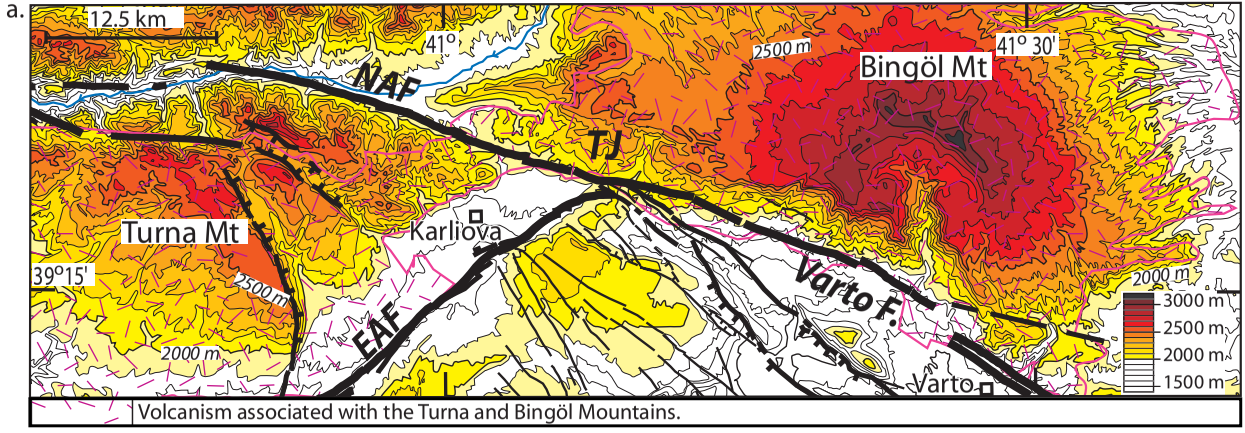

Volcanism associated with the Turna and Bingöl Mountains.

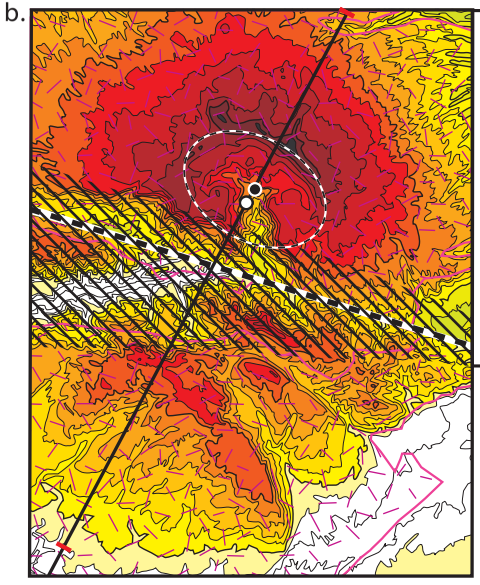

paleotopography not representative as hightly deformed by the NAF-Varto Fault system

mean direction of the NAF-Varto Fault system used in the restoration

ellipse defining the somital shape of the Bingol half-caldera

center of the Bingol half-caldera as defined by its somital shape

topographic section along the small axis of ellipse defining the shape of Bingol half caldera

center of reconstructed volcano as defined by the topographic section in c)

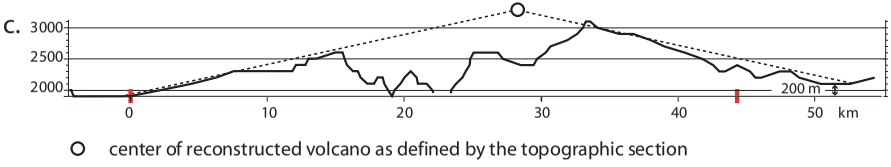

center of reconstructed volcano as defined by the topographic section

Figure 6

Figure 7

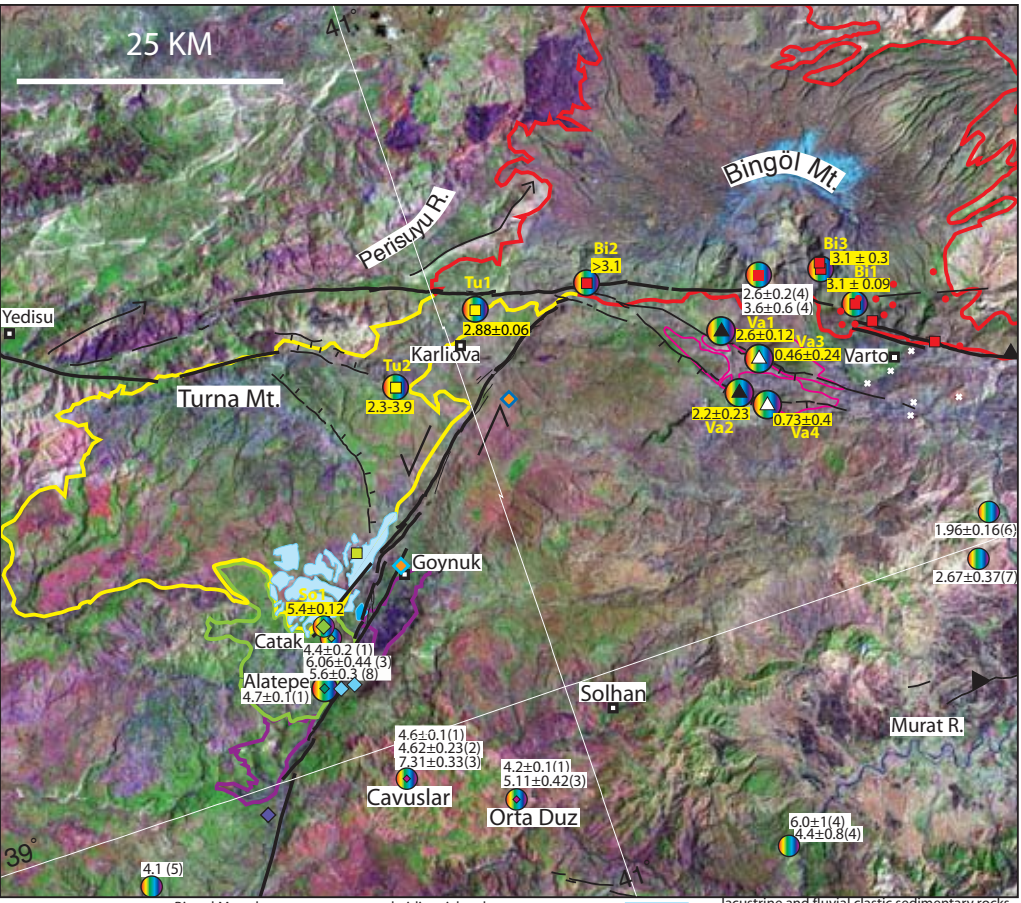

Bingol Mt. volc.
Turna Mt. volc.
obcidian rich volc
intrusive volc. related to Varto F.
offset metamorphic body along EAF
lacustrine and fluvial clastic sedimentary rocks interbedded with lava flows of the Turna Mt.
lignite deposit

Sample locations:
Bingol Mt. volc.
Pearce et al. (1990)'s Bingol volc.
Buket and Temel (1998)'s Bingol volc.
Turna Mt. volc

volc south of the Turna Mt.
obsidian samples of Catak and Alatepe (data from (4))
volc. EAF and south of offset metamorphic body
volc. west of EAF and south of offset metamorphic body

volc. east of EAF and south of triple junction
obsidian samples of Cavuslar/OrtaDuz (from (4)).
volcanism underlying fissural volcanism
fissural volcanism south of Bingol half-caldera
some Buket and Temel(1998)'s fissural volc

K-Ar, Ar-Ar and fission track ages : (1) Chataigner et al. 1998, (2) Bigazzi et al. 1997, (3) Poitevin et al. 1998, (4) Pearce et al. 1990, (5) Innocenti et al. 1982b, (6) Bigazzi et al. 1996, (7) Bigazzi et al. 1998, (8) Innocenti et al. 1982 a.

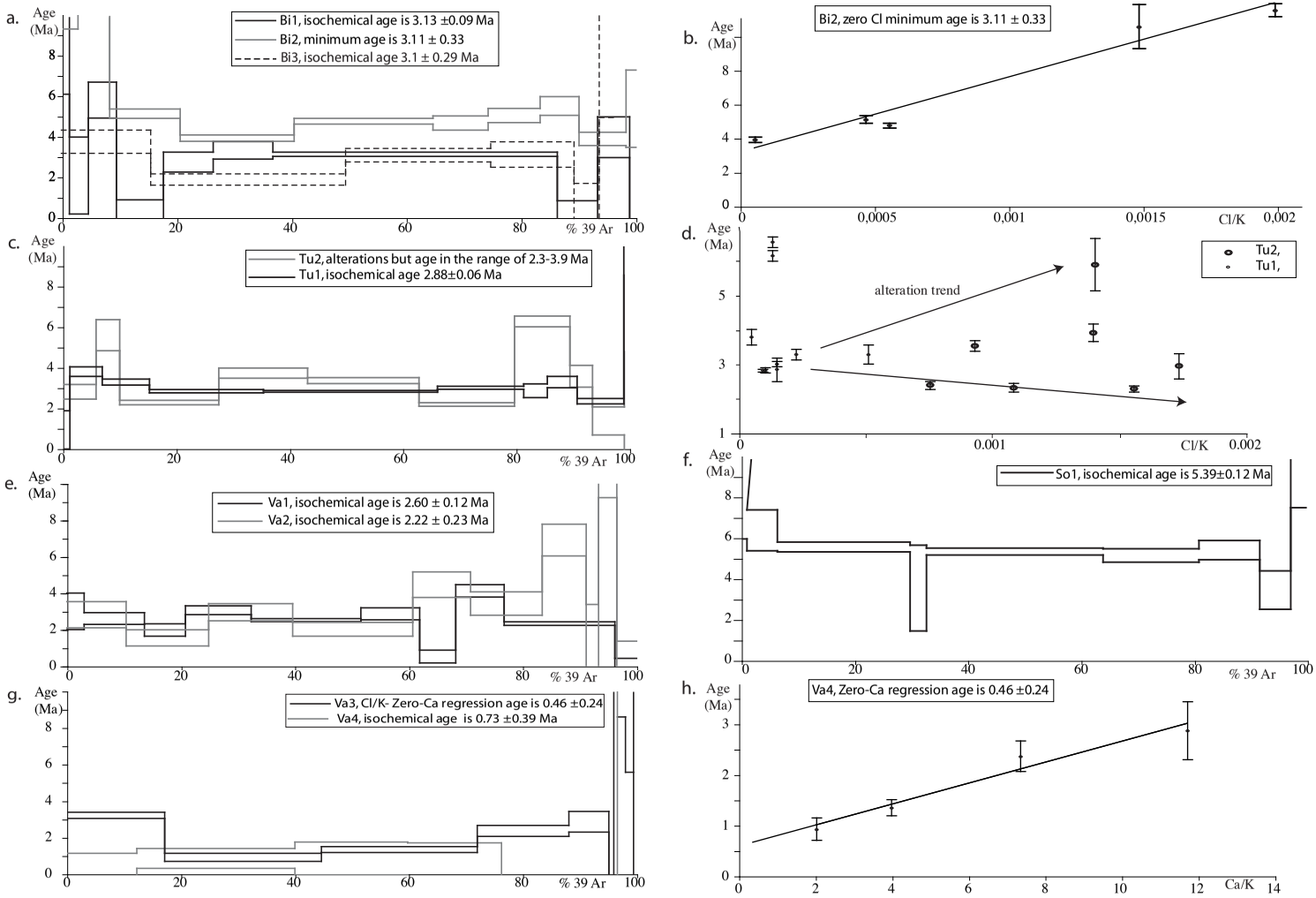
a.
Age (Ma)
Bi1, isochemical age is 3.13 ±0.09 Ma
Bi2, minimum age is 3.11 ± 0.33
Bi3, isochemical age 3.1 ± 0.29 Ma
% 39 Ar
b.
Bi2, zero Cl minimum age is 3.11 ± 0.33
Cl/K
c.
Tu2, alterations but age in the range of 2.3-3.9 Ma
Tu1, isochemical age 2.88±0.06 Ma
d.
Tu2,
Tu1,
alteration trend
e.
Va1, isochemical age is 2.60 ± 0.12 Ma
Va2, isochemical age is 2.22 ± 0.23 Ma
f.
So1, isochemical age is 5.39±0.12 Ma
g.
Va3, Cl/K- Zero-Ca regression age is 0.46 ±0.24
Va4, isochemical age is 0.73 ±0.39 Ma
h.
Va4, Zero-Ca regression age is 0.46 ±0.24
Ca/K

Figure 8

Figure 9 (1)

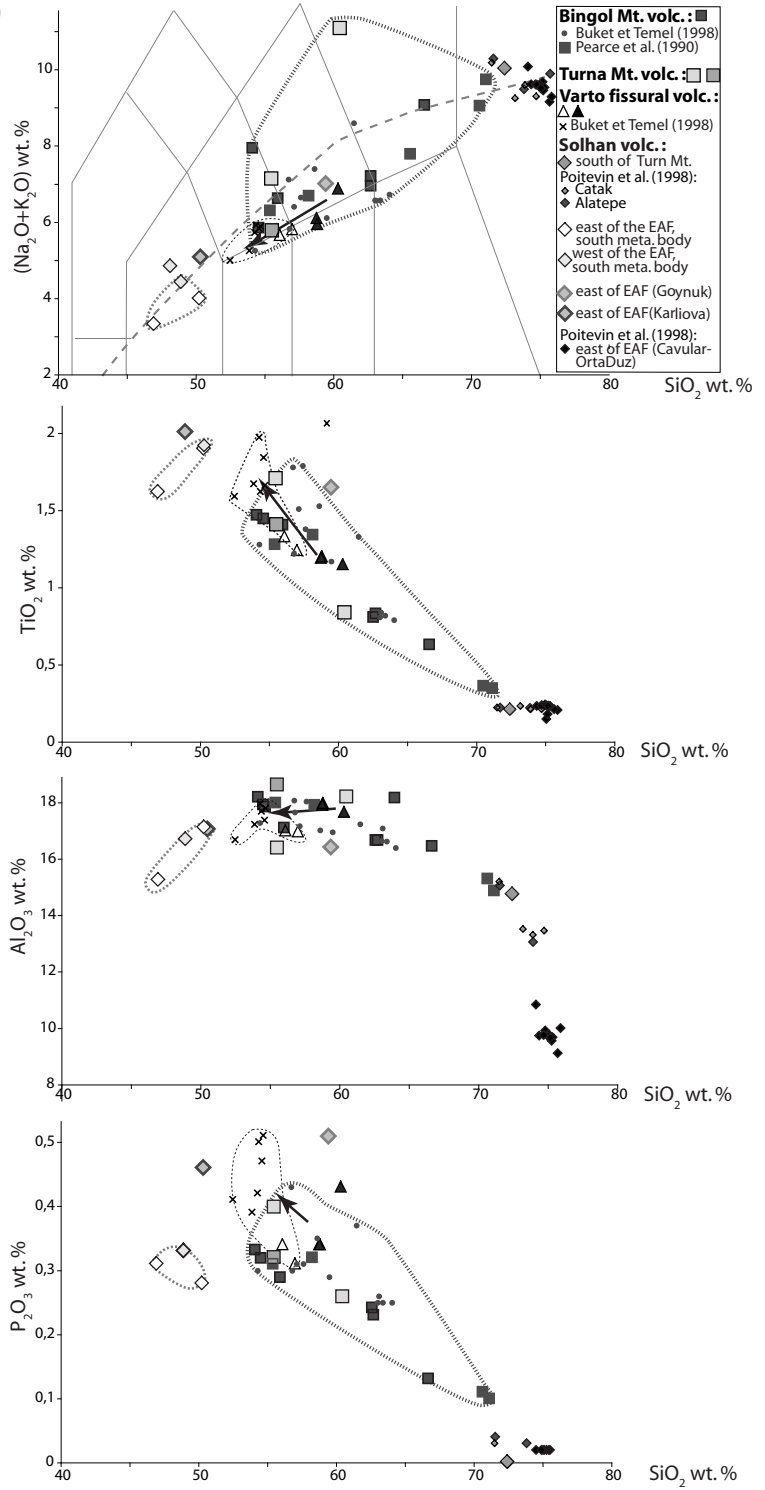
Bingol Mt. volc. :
Buket et Temel (1998)
Pearce et al. (1990)
Turna Mt. volc. :
Varto fissural volc. :
Buket et Temel (1998)
Solhan volc. :
south of Turn Mt.
Poitevin et al. (1998):
Catak
Alatepe
east of the EAF, south meta. body
west of the EAF, south meta. body
east of EAF (Goynuk)
east of EAF(Karliova)
Poitevin et al. (1998):
east of EAF (Cavular-OrtaDuz)
(Na2O+K2O) wt. %
SiO2 wt. %
TiO2 wt. %
Al2O3 wt. %
P2O3 wt. %

Figure 9 (2)

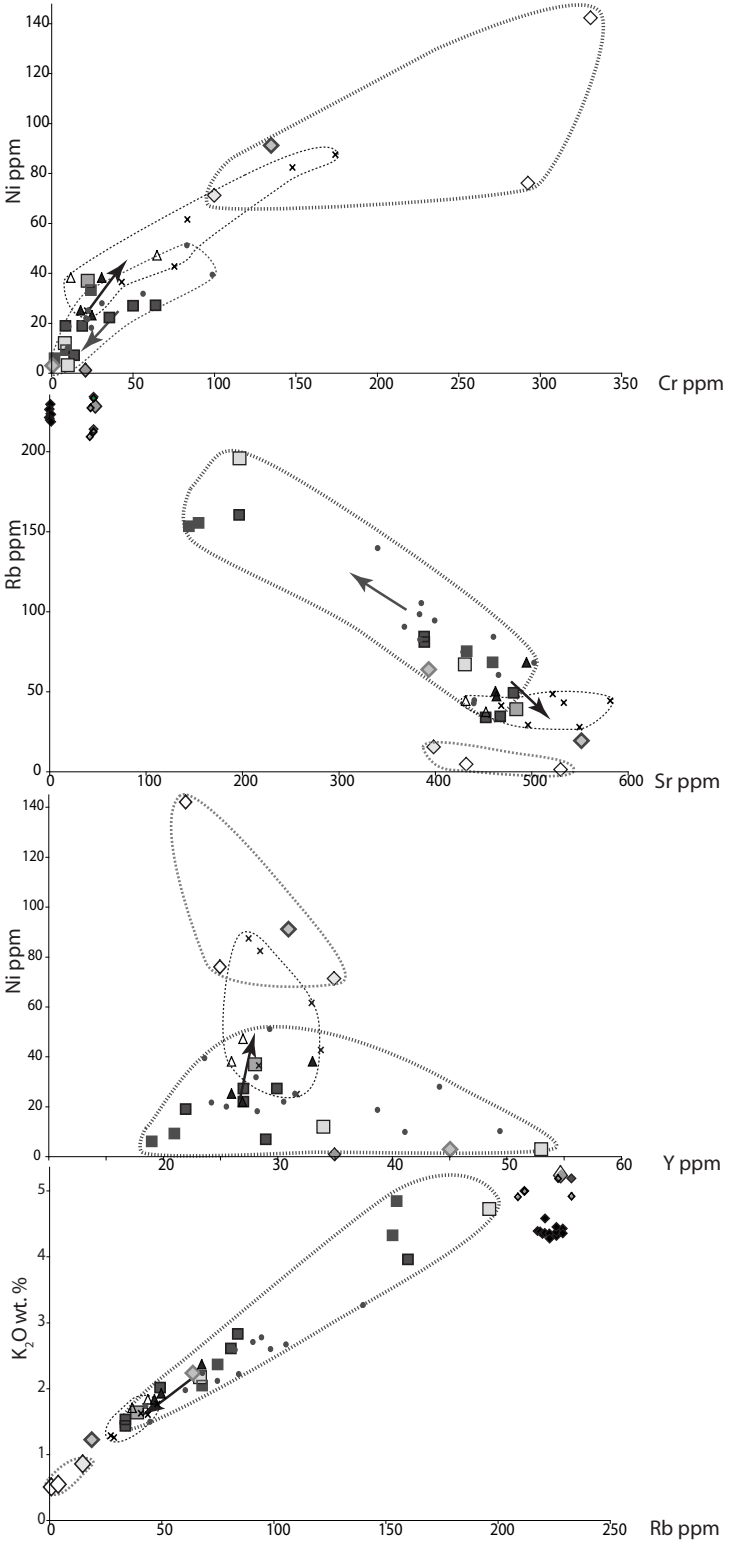

Figure 9 (3)

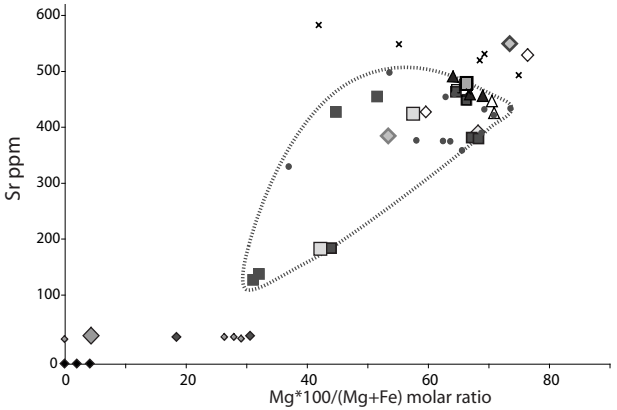
Sr ppm
600
500
400
300
200
100
0
0
20
40
60
80
Mg*100/(Mg+Fe) molar ratio

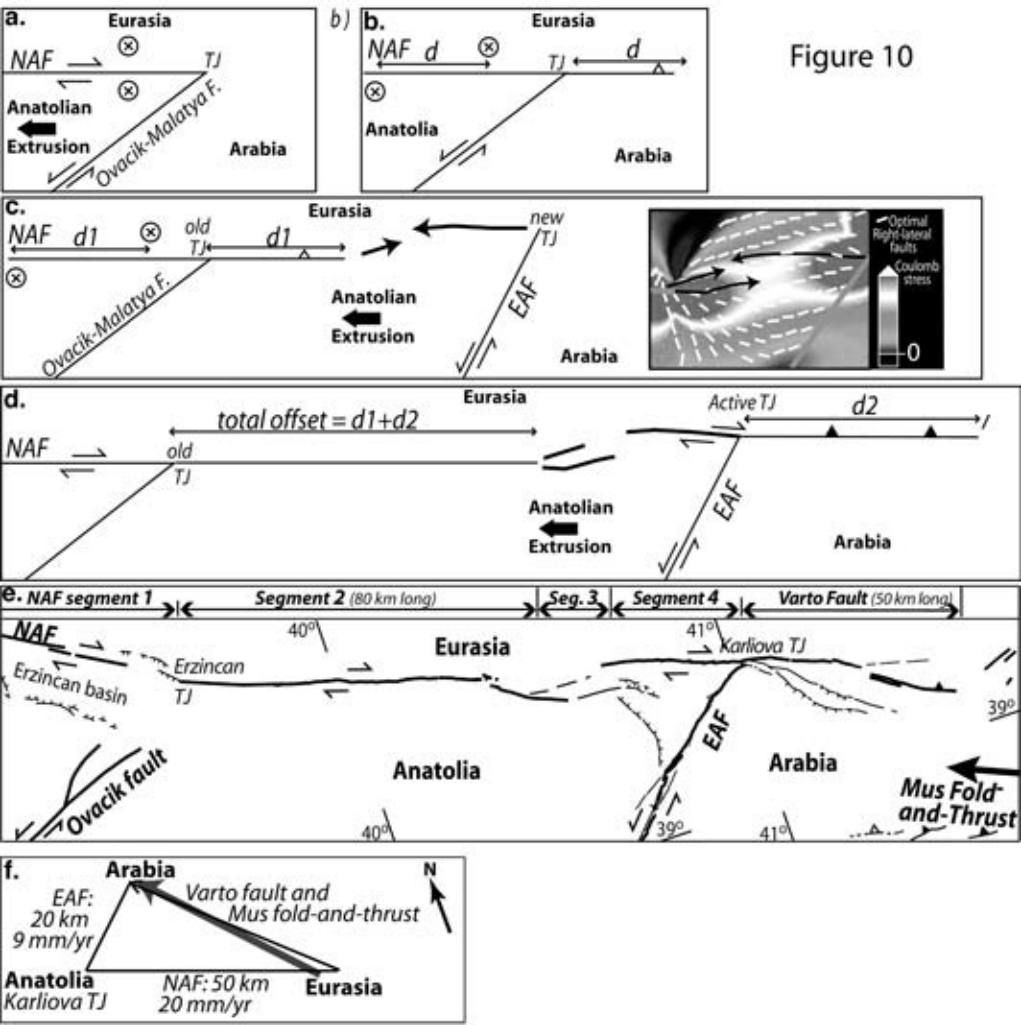
a.
Eurasia
NAF
TJ
Anatolian
Extrusion
Ovacik-Malatya F.
Arabia
b)
b.
Eurasia
NAF d
TJ
d
Anatolia
Arabia
Figure 10
c.
NAF d1
old TJ
d1
Eurasia
new TJ
Anatolian Extrusion
EAF
Ovacik-Malatya F.
Arabia
Optimal Right-lateral faults
Coulomb stress
0
d.
total offset = d1+d2
NAF
old TJ
Eurasia
Active TJ
d2
Anatolian Extrusion
EAF
Arabia
e.
NAF segment 1
Segment 2 (80 km long)
Seg. 3
Segment 4
Varto Fault (50 km long)
NAF
40°
Eurasia
41°
Karliova TJ
Erzincan basin
Erzincan TJ
39°
EAF
Ovacik fault
Anatolia
Arabia
Mus Fold-and-Thrust
40°
39°
41°
f.
Arabia
N
EAF: 20 km 9 mm/yr
Varto fault and Mus fold-and-thrust
Anatolia
Karliova TJ
NAF: 50 km 20 mm/yr
Eurasia

Figure 11

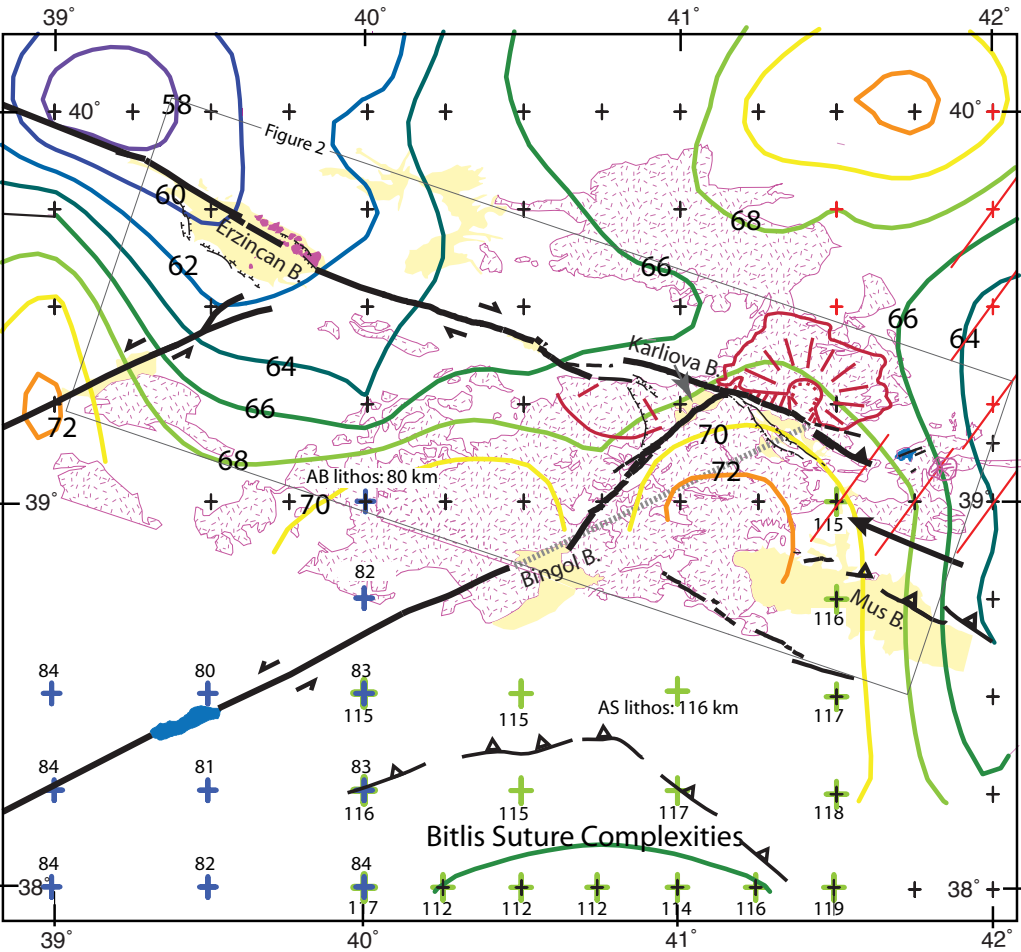

Depth of East Anatolian lithosphere - asthenosphere boundary (LAB) obtained by Angus et al (2006) using S-waves receiver function. Data points are extracted from published north-south and east-west profiles - LAB called East Anatolian accretionary complex and Rhodope-Pontide continental fragment in Angus et al. (2006)

Data points with a weak LAB signal

Low velocity zone (Angus et al. 2006)

Mean direction of the EAF, showing the strong 25˚ rotation of the Karliova segment

Interpolated East Anatolian LAB- Depth given in kilometers.

Depth of Arabian LAB obtained by Angus et al (2006) using S-waves receiver function. Data points are extracted from published north-south and east-west profiles - LAB called Arabian Shield LAB in Angus et al. (2006).

Depth of Anatolian LAB obtained by Angus et al (2006) using S-waves receiver function. Data points are extracted from published north-south and east-west profiles - LAB called Anatolian Block LAB in Angus et al. (2006).